Low-copy *piggyBac* transposon mutagenesis in mice identifies genes driving melanoma

Thomas K. Ni[a,1], Sean F. Landrette[a], Robert D. Bjornson[b], Marcus W. Bosenberg[c], and Tian Xu[a,d,2]

[a]Department of Genetics, Howard Hughes Medical Institute, and Boyer Center for Molecular Medicine, Yale University School of Medicine, New Haven, CT 06510; [b]Department of Computer Science and Yale Center for Genome Analysis, Yale University, New Haven, CT 06511; [c]Department of Dermatology, Yale University School of Medicine, New Haven, CT 06510; and [d]Institute of Developmental Biology and Molecular Medicine, Fudan–Yale Center for Biomedical Research, School of Life Science, Fudan University, Shanghai 200433, China

Edited by James E. Cleaver, University of California, San Francisco, CA, and approved August 9, 2013 (received for review July 30, 2013)

Despite considerable efforts to sequence hypermutated cancers such as melanoma, distinguishing cancer-driving genes from thousands of recurrently mutated genes remains a significant challenge. To circumvent the problematic background mutation rates and identify new melanoma driver genes, we carried out a low-copy *piggyBac* transposon mutagenesis screen in mice. We induced eleven melanomas with mutation burdens that were 100-fold lower relative to human melanomas. Thirty-eight implicated genes, including two known drivers of human melanoma, were classified into three groups based on high, low, or background-level mutation frequencies in human melanomas, and we further explored the functional significance of genes in each group. For two genes overlooked by prevailing discovery methods, we found that loss of membrane associated guanylate kinase, WW and PDZ domain containing 2 and protein tyrosine phosphatase, receptor type, O cooperated with the v-raf murine sarcoma viral oncogene homolog B (*BRAF*) recurrent V600E mutation to promote cellular transformation. Moreover, for infrequently mutated genes often disregarded by current methods, we discovered recurrent mitogen-activated protein kinase kinase kinase 1 (*Map3k1*)-activating insertions in our screen, mirroring recurrent *MAP3K1* up-regulation in human melanomas. Aberrant expression of *Map3k1* enabled growth factor-autonomous proliferation and drove *BRAF*-independent ERK signaling, thus shedding light on alternative means of activating this prominent signaling pathway in melanoma. In summary, our study contributes several previously undescribed genes involved in melanoma and establishes an important proof-of-principle for the utility of the low-copy transposon mutagenesis approach for identifying cancer-driving genes, especially those masked by hypermutation.

piggyBac PB transposon | somatic mutagenesis | low-copy genetic screen

The sequencing of human cancer exomes has led to the identification of new candidate driver genes with the understanding that genes promoting cancer growth (drivers) are more frequently mutated compared with genes not involved in cancer (passengers) (1). In addition, exome sequencing has uncovered the existence of hypermutated tumors, which possess greatly elevated background mutation rates (2–4). Nearly all melanomas and lung cancers are hypermutated, with an average of 433 and 256 nonsilent mutations per tumor, respectively (5–13). In these cancers, disproportionate increases in passenger mutations obfuscate the differential mutation frequencies used to distinguish drivers from passengers. Uncontrolled inflation of false-positive drivers obscures the identities of true drivers (low specificity) whereas overly stringent filters compromise the detection of true drivers (low sensitivity) (14). A productive balance between sensitivity and specificity remains to be achieved. Given these considerable challenges, efforts to identify genes important for hypermutated cancers would benefit from experimental cancer screens that can substantially reduce passenger mutations.

Since the mobilization of *piggyBac* (*PB*) and *Sleeping Beauty* (*SB*) transposons in mice (15, 16), transposon somatic mutagenesis screens have become important functional complements to human cancer sequencing (17–19). Prevailing high-copy *SB* insertional mutagenesis screens for cancer-gene discovery mobilize hundreds of transposons per cell to generate hundreds of insertional mutations, and this strategy has proven highly efficient at inducing tumors in mice. Although high insertional mutation rates present problems for distinguishing drivers from passengers similar to those seen in human cancers, high-copy screens use large cohorts of mice to achieve adequate statistical power for subsequent analysis. Although low specificity remains a serious issue, high-copy screens have identified several dozen genes whose human orthologs are frequently mutated in colorectal and pancreatic cancers (20–22).

For hypermutated cancers, the utility of such cross-species comparisons is limited due to the rampant mutation rates inherent in high-copy experimental mouse screens. In theory, the efficiency of *PB* transposition would permit screens for tumorigenesis to be performed using greatly reduced numbers of mutagenic transposons. The development of such low-copy mutagenesis systems would circumvent the insertional hypermutation produced by high-copy experimental mouse screens, thereby minimizing passenger mutations and enriching for potentially causative mutations. The virtue of such an approach would permit smaller cohorts of mice to be used and enable effective cross-species comparisons to further facilitate the identification of driver genes in human cancer.

We were intrigued by the potential of using limited numbers of transposons per cell for inducing tumors, as this approach has not previously been exploited. As proof-of-concept for the low-

Significance

Passenger mutation rates are highly elevated in many human cancers, posing a significant hurdle for the identification of cancer-driving genes. In this study, we screened for melanomas in mice using a unique, low-copy transposon mutagenesis system that can induce tumors with few somatic mutations. We show that our experimental system accurately recapitulated the genetic basis of human melanomas with only five somatic mutations, thus circumventing hundreds of unrelated passengers. Using cross-species comparative analyses and functional studies in human cells, we identified three previously undescribed genes involved in melanoma and several dozen candidate genes. Our study demonstrates that the low-copy transposon mutagenesis approach can facilitate the identification of cancer-driving genes that are masked by high passenger mutation rates.

Author contributions: T.K.N. and T.X. designed research; T.K.N. and S.F.L. performed research; R.D.B. and M.W.B. contributed new reagents/analytic tools; T.K.N., M.W.B., and T.X. analyzed data; and T.K.N. and T.X. wrote the paper.

The authors declare no conflict of interest.

This article is a PNAS Direct Submission.

[1]Present address: Department of Developmental, Molecular and Chemical Biology, Tufts University, Boston, MA 02111.

[2]To whom correspondence should be addressed. E-mail: tian.xu@yale.edu.

This article contains supporting information online at www.pnas.org/lookup/suppl/doi:10.1073/pnas.1314435110/-/DCSupplemental.

copy mutagenesis methodology, we set our sights on identifying new candidate genes for melanoma, the most hypermutated of human cancers. Melanomas often harbor driver mutations in *BRAF*, neuroblastoma RAS viral (v-ras) oncogene homolog (*NRAS*), cyclin-dependent kinase inhibitor 2A (*CDKN2A*), and phosphatase and tensin homolog (*PTEN*), as well as frequent amplifications but rare protein-coding mutations in microphthalmia-associated transcription factor (*MITF*) and v-kit Hardy-Zuckerman 4 feline sarcoma viral oncogene homolog (*KIT*) (23). However, knowledge of new driver genes remains limited. Using a low-copy *PB* mutagenesis system (seven-copy) in mice, we report the induction of melanomas with 100-fold lower mutation rates compared with human melanomas, the validation of *Cdkn2a* and *Mitf* as driver genes, and the identification of 36 previously undescribed candidate genes. By cross-species comparative analysis and experiments in human cells, we show that *MAGI2*, *PTPRO*, and *MAP3K1* have functional significance to human melanoma and are either overlooked or undetected by prevailing cancer-gene discovery methods. These findings demonstrate the power of low-copy transposon screens in mice for identifying genes relevant to human cancers, especially those with high mutation rates.

Results

Mouse Melanomas Induced by Few Somatic Mutations Recapitulate the Genetic Basis of Human Melanoma. In humans, benign nevi and malignant melanomas frequently harbor the oncogenic $BRAF^{V600E}$ mutation (24, 25). $BRAF^{V600E}$ is an important initiating mutation in melanoma but is insufficient for driving melanoma genesis on its own (26). To maximize the relevance of our experimental system to human melanoma, we used a conditional knock-in *Braf* mouse model, $Braf^{CA}$. In the presence of Cre recombinase, the functionally wild-type $Braf^{CA}$ allele is converted into $Braf^{V600E}$ (26, 27). We bred $Braf^{CA}$ mice with *Tyr-CreER* transgenic mice (28) to enable tamoxifen-inducible conversion of $Braf^{CA}$ specifically in melanocytes of double transgenic progeny. Two single transgenic lines (*Luc-PB[mut]7* and *Act-PBase*), each carrying half of the essential components of a low-copy *PB* somatic mutagenesis system that we previously developed (PB-SMART) (19), were separately crossed into this line. We then performed a forward genetic screen for melanomas by intercrossing triple transgenic mice (Fig. 1*A*). In this system, *PB* mutator transposons can be mobilized from their initial positions within luciferase reporter genes by the *PB* transposase (PBase) (Fig. 1*A*). Subsequent *PB* reinsertion at sites throughout the mouse genome can generate random insertional mutations that can drive or disrupt gene expression (Fig. 1*A*). The critical element of this approach is the restriction on the number of *PB* transposons per cell. By limiting each cell to seven mutator transposons, we ensure that no cell can concurrently harbor more than seven insertions.

A luciferase-labeled mutagenesis cohort of mice that mobilize *PB* mutator transposons in somatic cells ($Braf^{CA}$*;Tyr-CreER;Luc-PB[mut]7;Act-PBase*) and a nonmutagenesis control cohort ($Braf^{CA}$*;Tyr-CreER;Luc-PB[mut]7* or $Braf^{CA}$*;Tyr-CreER;Act-PBase* littermates) were monitored for the development of melanomas. Beginning 4 mo after activating oncogenic *Braf*, luciferase-expressing tumors formed in the mutagenesis cohort and were confirmed to be malignant melanomas by histology and immunohistochemistry (Fig. 1 *B–E*). Overall, 8/17 mice in the mutagenesis cohort succumbed to melanomas within 15 mo whereas the control cohort remained mostly melanoma-free (Fig. 1*F*), indicating that the seven-copy *PB* mutator drove the development of melanoma.

We performed linker-mediated PCR and Illumina sequencing to comprehensively map the insertional landscape in melanomas from our mutagenesis cohort as well as three *PB*-induced melanomas from other low-copy (seven-copy) mutagenesis screens not using $Braf^{V600E}$. Sixty percent of insertions were located in transcription units or genes (hereafter referred to as insertional mutations), and the rest were intergenic. We noted that very few insertional mutations accounted for the vast majority of sequencing reads within each tumor. The preponderance of reads from these insertions likely reflects their clonal abundance in the melanomas and thus identifies them as potential driver mutations. Random sampling of one-third of all insertional mutations by genomic PCR confirmed the clonal abundance of mutations (Fig. S1). In total, 45 insertional mutations in 38 genes (37 protein-coding, 1 noncoding RNA) were identified, corresponding to an average of 4.1 insertional mutations per tumor (Table S1).

Importantly, among the identified genes are two bona fide melanoma driver genes, *Mitf* and *Cdkn2a*. *MITF* is a melanocyte lineage-restricted oncogene that is frequently amplified in human melanomas (23). Consistent with the alterations in human melanomas, we found that mouse melanomas harboring insertional mutations in *Mitf* were up-regulated approximately sevenfold by real-time RT-PCR (qPCR) (Fig. 1*G*). Meanwhile, *CDKN2A* is a tumor suppressor gene frequently mutated or deleted in human melanomas (23), and, in a mouse melanoma, we likewise mapped an insertional mutation disrupting the third exon of *Cdkn2a* (insertion in the 3′ UTR of $p16^{Ink4a}$ and $p19^{Arf}$). Using primers capable of detecting both products expressed by the *Cdkn2a* locus, we found that the insertional mutation reduced gene expression within the tumor (Fig. 1*H*). Combined with the $Braf^{V600E}$ mutation used at the outset of the screen, our identification of *Cdkn2a* and *Mitf* covers 50% of all functionally verified melanoma drivers, providing strong validation for the relevance of this screen to human melanoma and for investigating the yet-to-be-identified oncogenic events necessary for melanoma.

Given an average of four insertional mutations per tumor, the probability of multiple insertions in the same gene across melanomas occurring due to chance is extremely low, suggesting that recurrent mutations are highly likely to drive melanoma. We identified *Mitf*, *Arhgef3*, *Map3k1*, *Map3k2*, and *Rapgef2* as recurrently mutated genes (Table 1), highlighting the potential importance of four previously undescribed genes in promoting melanomas. The high frequency of coding-direction insertional mutations affecting *Arhgef3*, which encodes a regulator of Rho family GTPases, and significant enrichment for genes involved in Rho family GTPase signaling as identified by Ingenuity Pathway Analysis ($P = 0.01$, Benjamini–Hochberg method for multiple testing) support a role for hyperactive Rho family GTPase signaling in melanoma. Notably, these results are consistent with recent discoveries that Rho family GTPases are recurrently activated in human melanomas (10, 11). Multiple coding-direction insertional mutations were also recovered in *Rapgef2* and *Rap2b*, suggesting that Rap GTPases may promote tumor formation.

Two important proofs-of-principle are established by these results. First, low-copy *PB* insertional mutagenesis can efficiently induce solid tumors such as melanomas in mice. Second, this system can be used to identify true human driver genes. Furthermore, because the low-copy *PB* system minimizes the accumulation of unrelated passenger mutations, it is poised to facilitate the discovery of new genes associated with cancer, especially hypermutated cancers.

Identification of Recurrent and Mutually Exclusive *Map3k1/2* and $Braf^{V600E}$ Mutations in Melanomas. Given that multiple random insertions into the same gene across multiple melanomas using this low-copy mutagenesis strategy is extremely unlikely, we postulated that frequently mutated genes from our screen are functionally important for melanoma. Of the 38 genes, Map-3-kinase family members were the most frequently mutated. Transposon insertions in *Map3k1* were clustered in introns 9 and 10 (Fig. 2*A*), despite no enrichment of *PB* target sites in the region. All three insertions were oriented in the coding direction, suggesting over-

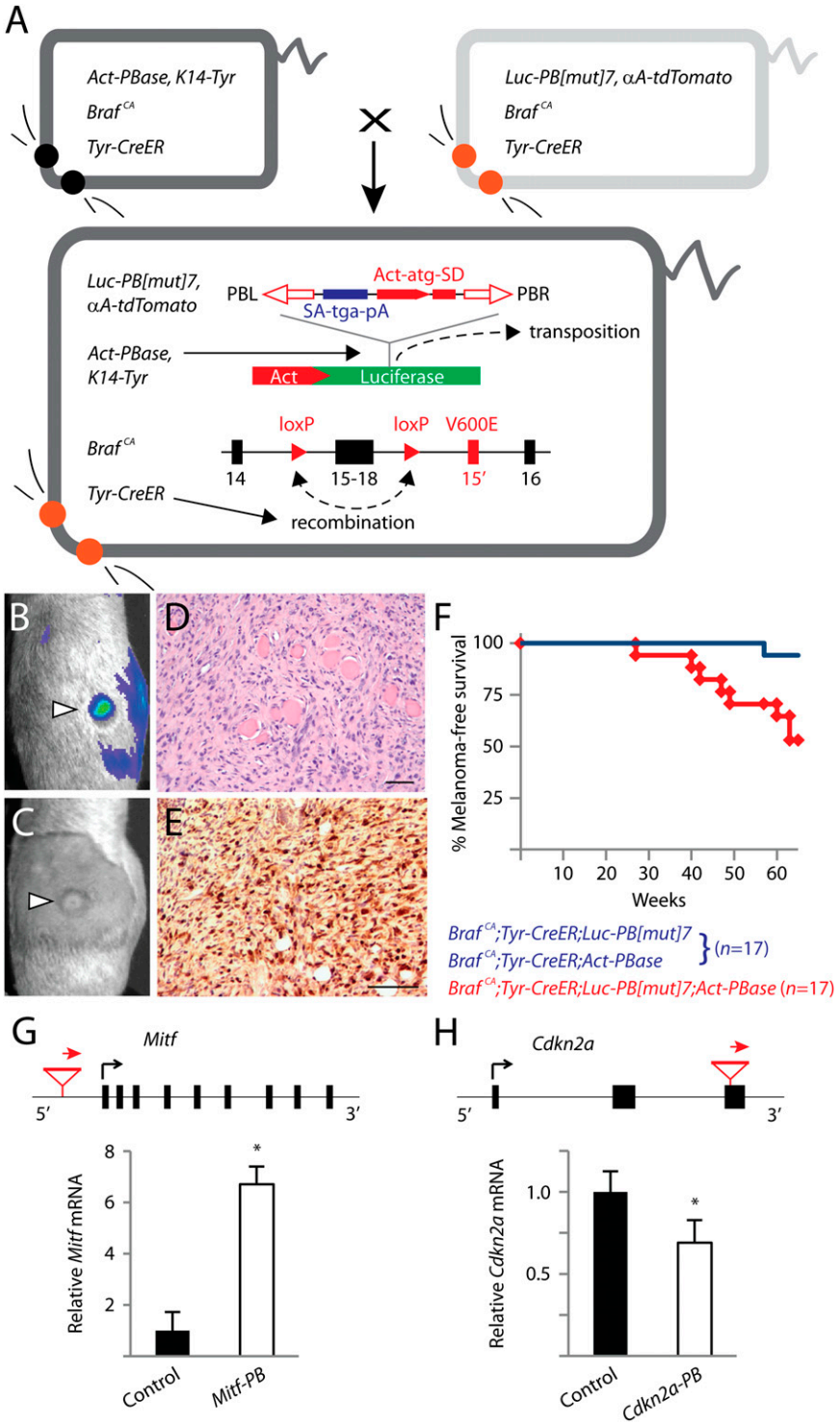

Fig. 1. Low-copy *PB* somatic mutagenesis induces malignant melanomas that recapitulate the known genetic basis of human melanoma. (*A*) The low-copy forward genetic screen uses an inducible, melanocyte-specific somatic mutation in *Braf* (*Braf*^{V600E}) and *PB* somatic insertional mutagenesis. *PB[mut]* carries a splice acceptor, stop sequence, and poly-A signal, as well as an Actin promoter driving an initiator exon with splice donor sequence. *PB[mut]* is initially inserted in the luciferase gene, and, upon "cut-and-paste" transposition mediated by PBase, the mutator transposon can integrate into sites in the host genome. Precise reconstitution of the luciferase gene following transposition permits the labeling of melanomas (*B*) that develop following tamoxifen administration (*C*). Melanomas induced by *PB[mut]* are highly invasive, seen here invading through muscle (*D*), and display positive immunoreactivity to the S100 melanoma marker (*E*). (Scale bars: *D* and *E*, 50 μm.) (*F*) Mice in the mutagenesis cohort developed melanomas significantly earlier than mice in the control cohort ($P < 0.005$, log-rank test). (*G*) An insertion into the promoter region of *Mitf* led to a sevenfold up-regulation of gene expression, consistent with the known role of *MITF* as an oncogene. (*H*) An exon-interrupting insertion found in the tumor suppressor gene *Cdkn2a* reduced mRNA expression. Relative transcript levels in melanomas with *Mitf* or *Cdkn2a* insertional mutations were compared with three melanomas not harboring these insertions. *$P < 0.05$, *t* test. Data in *G* and *H* are presented as mean ± SD ($n = 3$).

Table 1. Recurrently mutated genes found in low-copy *PB* mutagenesis screen

Gene symbol	No. tum	Location	Orientation	Gene name
Arhgef3	3	Intron 2	Coding	Rho guanine nucleotide exchange factor (GEF) 3
Map3k1	3	Introns 9 and 10	Coding	Mitogen-activated protein kinase kinase kinase 1
Map3k2	2	Intron 5	Coding	Mitogen-activated protein kinase kinase kinase 2
Mitf	2	5′ regulatory region	Coding	Microphthalmia-associated transcription factor
Rapgef2	2	Intron 1	Coding	Rap guanine nucleotide exchange factor (GEF) 2

Location, the gene region affected by insertional mutations; No. tum, the number of tumors affected by insertional mutations in the gene; Orientation, the direction of the *PB* mutator cassette relative to gene transcription.

expression of the 3′ gene portion (Fig. 2*A*). RT-PCR with primer pairs spanning the *PB* mutator transposon's initiator exon (Fig. 1*A*) and downstream *Map3k1* exons confirmed the presence of chimeric *PB-Map3k1* transcripts (Fig. 2*B*). An overall increase of *Map3k1* transcript levels was observed in mutated tumors by qPCR (Fig. 2*C*). Overexpression of Map3k1 in these tumors was verified by immunohistochemistry using an antibody directed against the C-terminal region of Map3k1 (Fig. 2*D*). Similarly, insertions in *Map3k2* were regionally clustered (Fig. 2*A*), induced the expression of chimeric *PB-Map3k2* mRNA (Fig. 2*B*), and drove overexpression (Fig. 2*C*). The recurrent mutation and overexpression of *Map3k1/2* gene products suggest a functional importance in melanoma.

Seventy percent of human melanomas harbor oncogenic *BRAF* or *NRAS* lesions that constitutively activate ERK signaling (23). When overexpressed in cultured cells, Map3k1/2 can also activate ERK signaling (29, 30); however, these genes have not been previously implicated in melanoma. Recurrent mutations causing *Map3k1/2* overexpression were surprising given that the somatic $Braf^{V600E}$ mutation used in the screen already drove ERK signaling. We surmised that these mutations may have arisen in rare melanocytes retaining $Braf^{CA}$. The conditional *Braf* allele made it possible to examine whether *Braf* was oncogenically activated in *Map3k1/2*-mutated melanomas. Indeed, we found that $Braf^{V600E}$ and *Map3k1/2* mutations were mutually exclusive in all but one melanoma (Fig. 2*E*). An additional *Map3k1* mutation was isolated from a $Braf^{WT}$ melanoma, confirming that the majority of *Map3k1/2* insertional mutations occurred in melanocytes retaining functionally wild-type *Braf*. We mapped the predicted gene products of the *Map3k1* insertional mutations and discovered that they included the kinase domain but removed an E3 ubiquitin ligase domain that negatively regulates ERK signaling (Fig. 2*F*) (31). These data suggest that the *Map3k1* insertional mutations may act in a similar manner to oncogenic *Braf* by constitutively activating ERK signaling.

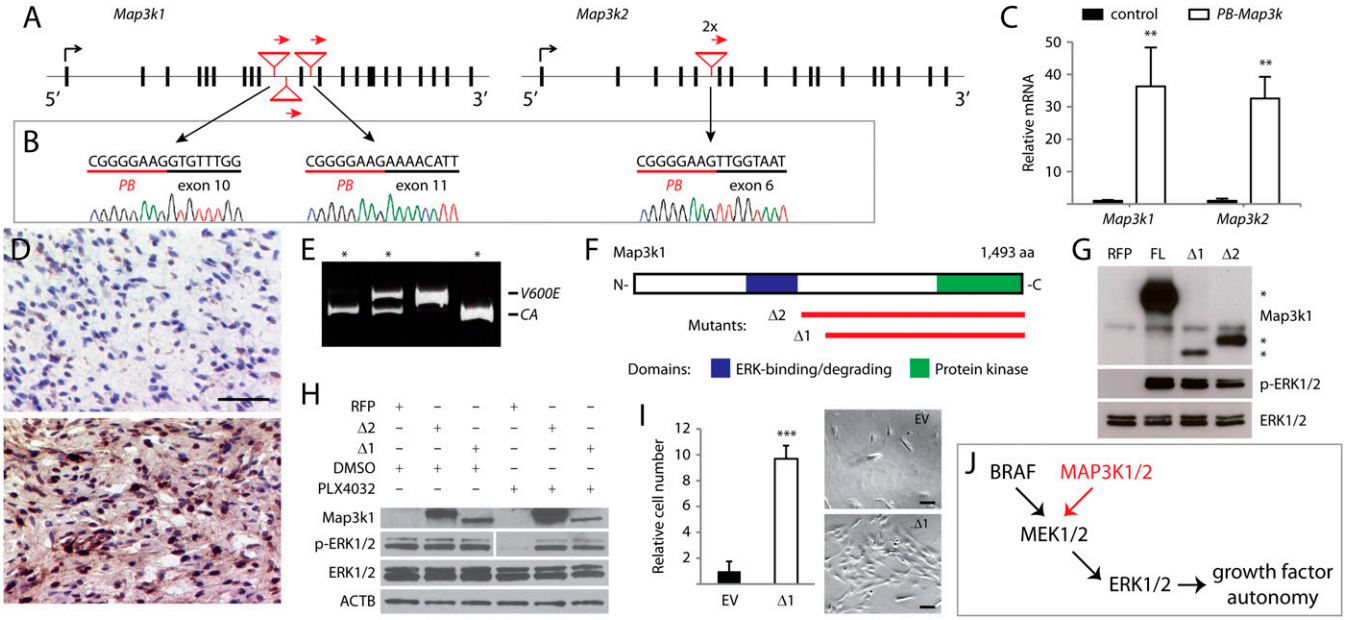

Fig. 2. Recurrent insertional mutations in *Map3k1/2* activate ERK signaling. (*A*) Insertional mutations oriented in the coding direction clustered in introns 9 and 10 of *Map3k1* and in intron 5 of *Map3k2*. (*B*) Chimeric *PB-Map3k1* and *PB-Map3k2* mRNA are detected by RT-PCR. (*C*) *Map3k1* and *Map3k2* transcripts are highly up-regulated in mutated versus nonmutated tumors. Relative transcript levels in melanomas with *Map3k1* or *Map3k2* insertional mutations were compared with three melanomas not harboring these insertions. $^{**}P < 0.05$, *t* test. (*D*) Immunohistochemistry confirmed higher expression in *Map3k1*-mutated melanomas (*Lower*) versus control melanomas (*Upper*). (Scale bar: 25 μm.) (*E*) Two-thirds of *Map3k1/2* mutations in the $Braf^{CA}$ background are mutually exclusive with $Braf^{V600E}$ as determined by genomic PCR (*Map3k1/2*-mutated tumors marked by *). (*F*) MAP3K1 protein domains and aberrant gene products (red lines) are depicted. (*G*) HEK293T cells transfected with full-length or aberrant *Map3k1* activate ERK in contrast to control cells transfected with *RFP* (Map3k1 protein bands denoted by *). (*H*) PLX4032 treatment abrogates ERK phosphorylation in control-transfected human YUMAC melanoma cells but not in cells expressing aberrant *Map3k1*. Light and dark exposures are shown for phospho-ERK in DMSO- and PLX4032-treated lanes, respectively. (*I*) The 10× increase in p′mel cells expressing $Map3k1^{\Delta 1}$ versus cells transduced with empty vector (EV) following growth factor deprivation. $^{***}P < 0.0001$, *t* test. (Scale bars: 100 μm.) (*J*) Model depicting how *Map3k1/2* activation in $Braf^{WT}$ melanomas can activate ERK signaling to confer growth factor-autonomous survival and proliferation. Data in *C* and *I* are presented as mean ± SD ($n = 3$).

To test this hypothesis, we generated the aberrant Map3k1 products (Map3k1$^{\Delta 1/2}$) and found that their exogenous expression in HEK293T cells efficiently activated ERK signaling as determined by antibody conjugation to phosphorylated ERK1/2 (Fig. 2*G*). We further interrogated the *Map3k1* mutations for ERK-activating ability in the YUMAC human melanoma cell line, which harbors homozygous oncogenic *BRAF*^{V600K} mutations (32). To determine the contribution of aberrant *Map3k1* to ERK activation in these cells, BRAF-induced ERK phosphorylation was suppressed by treatment with the oncogenic BRAF-inhibitor PLX4032 (Fig. 2*H*). Strikingly, YUMAC cells expressing Map3k1$^{\Delta 1/2}$ sustained ERK activation in the presence of PLX4032 (Fig. 2*H*), demonstrating that the ability to drive ERK activation is independent of BRAF.

Although oncogenic *BRAF* cannot initiate melanoma without cooperating mutations (26), it confers important malignant hallmarks such as the ability to proliferate independent of growth factors (33). We investigated whether aberrant *Map3k1* can also confer growth factor independence to nontransformed p'mel human melanocytes (33). Melanocytes expressing activated Map3k1 proliferated under growth-factor deprivation whereas vector-transduced p'mel cells underwent cell death or stopped proliferating (Fig. 2*I*).

Taken together, our data indicate that aberrant *Map3k1* leads to elevated ERK signaling (Fig. 2*J*), which can contribute to melanoma initiation by driving melanocyte proliferation irrespective of upstream growth factor signals. Thus, by using the low-copy *PB* mutagenesis strategy, we have uncovered an alternative means of activating ERK signaling in melanoma that is independent of the known driver gene *BRAF*.

Identification of a Highly Mutated Network Surrounding *MAGI2*. In one tumor harboring only three insertional mutations, we discovered that the recurrently mutated *Rapgef2* cooccurred with an insertional mutation affecting *Magi2*. *Magi2* encodes a multiple-PDZ domain-containing scaffolding protein that physically interacts with Rapgef2 (34) and also binds to other proteins frequently mutated in cancer, including the tumor suppressor PTEN and the oncogene β-catenin/CTNNB1 (Fig. 3*A*) (35, 36). Although *MAGI2* itself has not been previously implicated as a driver gene, the striking cooccurrence of *Rapgef2* and *Magi2* insertional mutations in our low-copy screen and the network of putative protein associations suggest that *MAGI2* might be important for melanoma.

In the mouse tumor harboring the insertional mutation, we observed greater than 50% reduction in *Magi2* gene expression (Fig. 3*B*). To evaluate the importance of *MAGI2* for melanocyte malignancy, we used p'mel cells expressing BRAF^{V600E}, which remain nontransformed (33). Lentivirus-mediated short hairpin RNA interference of *MAGI2* (Fig. 3 *C* and *D*) strikingly promoted anchorage-independent growth of p'mel-BRAF^{V600E} cells in soft agar assays compared with cells expressing scrambled control shRNA (Fig. 3 *E* and *F*). These results, taken together with the mutagenesis data in mice, indicate that loss of *MAGI2* can cooperate with oncogenic *BRAF* mutation to promote cellular transformation.

High background mutation rates in human melanomas have made it difficult to distinguish cancer-causing genes from passengers. To determine whether *MAGI2* is disrupted in human melanoma patients, we examined mutation data from six melanoma exome sequencing studies and found that *MAGI2* is frequently mutated (8.1% of 298 patients) (6–11). However, despite our evidence demonstrating the functional importance of *MAGI2*, the frequency of nonsilent mutations in this gene was not significantly higher than the background mutation rate (Fig. 3*G*; P = 0.119, χ^2 test). We suspected that this driver might be masked by high rates of passenger mutations in melanoma, thus preventing appropriate identification by prevailing methods without considerably more mutation data. Indeed, when we increased the statistical power of the sequencing dataset by analyzing mutation data across 272 additional melanoma exomes from The Cancer Genome Atlas (TCGA), we were able to detect the significance of *MAGI2* mutation burden (Fig. 3*G*; P = 0.011, χ^2 test). Moreover, two whole-genome sequencing studies have uncovered potentially frequent deletions and inversions (15.4%) affecting the *MAGI2* locus (5, 9). *MAGI2* and the closely-related *MAGI3* have also been discovered to harbor rearrangements in prostate and breast-cancer patients (37, 38). Altogether, the findings that have emerged from our low-copy *PB* mutagenesis screen and the correlation with human mutation data indicate that the disruption of *MAGI2* is likely a previously unrecognized but clinically relevant event in human melanoma and potentially other human cancers.

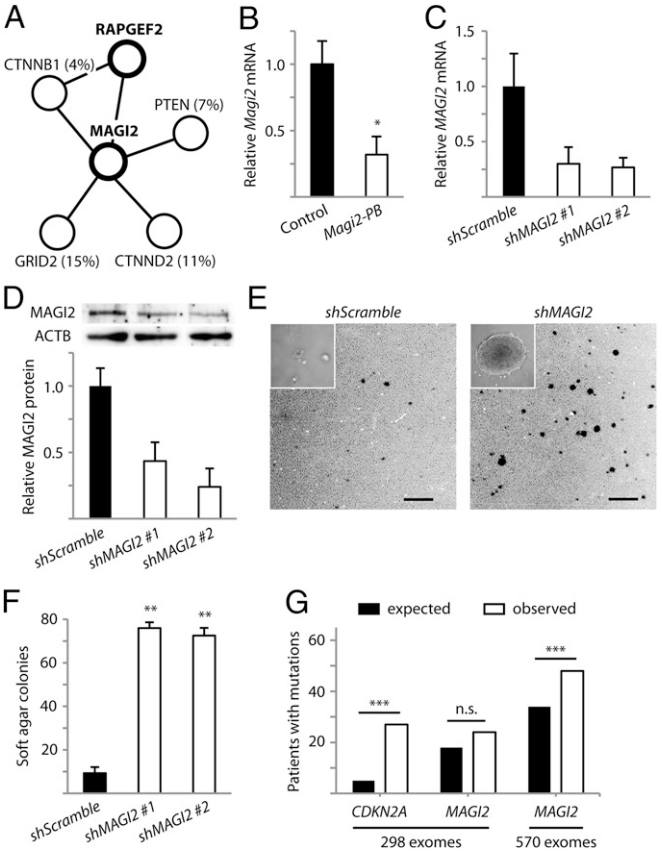

Fig. 3. Disruption of *MAGI2* promotes transformation of melanocytes. (*A*) A protein interaction network surrounding *MAGI2* is frequently mutated by *PB* insertions in mice (thick circles) and somatic point mutations in humans (thin circles, percentages of patients provided in parenthesis). (*B*) Insertional mutation reduced *Magi2* gene expression in a mouse tumor. Relative *Magi2* transcript levels in the insertionally mutated melanoma were compared with three melanomas not harboring *Magi2* insertion. *$P < 0.05$, *t* test. Expression of shRNA constructs for *MAGI2* diminish mRNA (*C*) and protein levels (*D*) in human p'mel-BRAF^{V600E} melanocytes. Cells expressing scramble shRNA were used as controls. (*E*) Depletion of *MAGI2* in p'mel-BRAF^{V600E} melanocytes promotes soft agar colony formation. Representative soft agar fields are shown. *Inset* displays high-powered image of a representative soft agar colony. (Scale bars: 1 mm.) (*F*) Colonies greater than 100 μm in diameter are quantified. **$P < 0.0001$, *t* test. (*G*) Detected nonsilent mutations for *CDKN2A* and *MAGI2* are displayed versus expected background mutations for genes of identical sizes. ***$P < 0.05$, χ^2 test. Data in *B*, *C*, *D*, and *F* are presented as mean ± SD ($n = 3$).

Low-Copy *PB* Mutagenesis Implicates Cancer-Associated Genes with Broad Spectrum of Mutation Burdens. Cross-species comparisons between high-copy mutagenesis results and hypermutated cancer-

exome sequencing data are problematic because the rampant background mutation rates intrinsic to the tumors from both species inflate false-positive drivers. On the other hand, a low-copy mutagenesis approach, which minimizes the accumulation of passenger mutations, may serve as a potent predictor of potential driver genes that cannot simply be discovered by repeatedly sequencing tumors and would therefore be highly amenable for cross-species comparative analysis.

We found extensive intersections by cross-species comparison of our genes to melanoma patient mutation data from six whole-exome sequencing studies, the Catalogue of Somatic Mutations in Cancer (COSMIC), and TCGA (6–11, 39). Six genes are mutated in 75% of the human sequencing datasets; more than half of the 38 genes are mutated in at least 4 datasets (Fig. 4*A*). Every gene identified in our screen is mutated in human melanomas, with many mutated in multiple patients (Table S2). Eight genes are also affected by intragenic break points from structural rearrangements (Table S2) (9). The high degree of intersection between our mouse melanoma drivers and human melanoma mutation data is consistent with the possibility that these genes may be important for human melanoma.

By accounting for the size of a gene and the average number of nonsilent mutations in human melanomas, the probability of random mutation occurring in any gene can be estimated (*Materials and Methods*). Using this model, we calculated the background mutation frequencies for the human ortholog of each gene identified in our screen. We subsequently compared them with empirical mutation frequencies in 570 human melanomas. From this analysis, the genes separated into three groups according to mutation burden (Fig. 4*B* and Table S2). Five genes are mutated at significantly higher frequencies compared with background (group I), and, among these, the melanoma tumor suppressor *CDKN2A* is the most significantly mutated gene. Along with *MAGI2*, three other genes (*PCDH15*, *MYF6*, and *CORIN*) are also mutated at statistically significant frequencies (Fig. 4*B*). Although these candidate genes have not previously been implicated by human melanoma sequencing studies, they are in fact distinguishable from passengers when data from all studies are analyzed in aggregate. Thus, the identification of group I genes by both low-copy *PB* mutagenesis and whole-exome sequencing indicates that they may be drivers of human melanoma.

Because we were interested to determine whether our approach can identify driver genes that cannot be discovered by prevailing methods, we next focused on genes that are mutated at significantly lower frequencies than background (group II). Genes with low somatic mutation burdens are often disregarded by cancer exome sequencing studies. However, group II genes were identified by our low-copy screen, which should have minimized the accumulation of passenger mutations. We therefore reasoned that at least some of these genes are nevertheless likely to be important for melanoma. For example, a low mutation burden may reflect the propensity for somatic mutations in a putative protooncogene to interfere with, rather than aberrantly activate, a vital function in melanoma cells, resulting in negative selection of mutations in these genes. In support of our reasoning, *MITF* is a member of this group as it is frequently amplified in melanoma (33) and infrequently disrupted by protein-coding mutations due to its importance to the melanocyte lineage (Fig. 4*B*) (23).

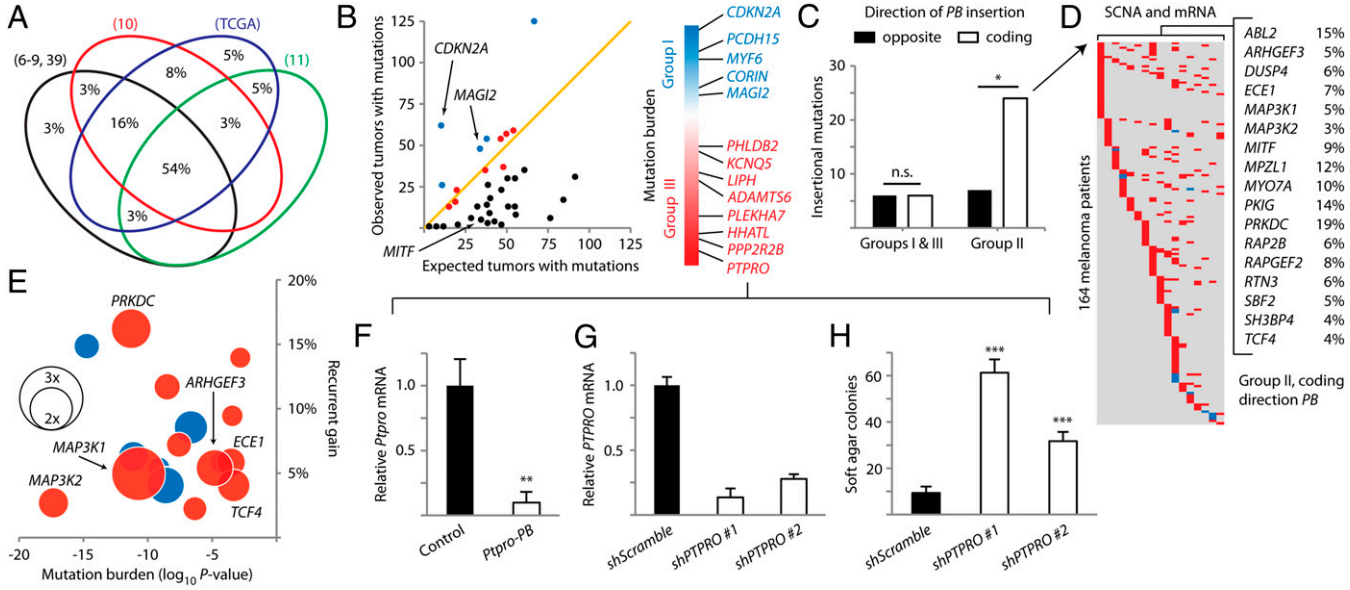

Fig. 4. *PB*-implicated genes have a wide spectrum of mutation frequencies in human melanoma. (*A*) Venn diagram shows the substantial overlap between genes identified in the low-copy *PB* screen and genes mutated in eight human melanoma mutation datasets (depicted as four ellipses, with the four smallest datasets grouped as one ellipse in black). (*B*) The detected mutation burden of each gene is plotted against the expected background mutation burden for genes of corresponding sizes. The orange line marks a 1:1 ratio of observed versus background. Genes are colored by group (group I, blue; group II, black; group III, red). Genes in groups I and III are ordered according to the significance of their mutation burdens. (*C*) The 4× enrichment of coding direction *PB* insertions is observed in group II genes, predicting overexpression. $*P < 0.005$, χ^2 test. (*D*) Copy number and expression data for genes enriched in *C* show significant alterations in 164 out of 222 melanoma patients (amplification/up-regulation in red, deletion/down-regulation in blue). (*E*) Bubble chart plotting genes from *D* by significance of mutation burden (*x* axis, negative values indicate low mutation burden versus background) and percentage of patients with recurrent gains or losses (*y* axis, positive values indicate percentage of patients with recurrent gain). Expression changes in melanomas relative to normal melanocytes are plotted as bubbles (up-regulation in red, down-regulation in blue). (*F*) *Ptpro* expression is diminished in a mouse melanoma harboring insertion in the gene. Relative *Ptpro* transcript levels in the insertionally mutated melanoma were compared with three melanomas not harboring *Ptpro* insertion. $**P < 0.001$, *t* test. (*G*) shRNA constructs reduced *PTPRO* mRNA levels in p′mel-BRAF^{V600E} cells. (*H*) Depletion of *PTPRO* in p′mel-BRAF^{V600E} cells promoted soft agar colony formation. Colonies greater than 100 μm in diameter are quantified. $***P < 0.0001$, *t* test. Data in *F*, *G*, and *H* are presented as mean ± SD ($n = 3$).

Interestingly, we observed a significant enrichment in coding-oriented *PB* insertional mutations affecting group II genes (Fig. 4*C*; P = 0.001, χ^2 test). In fact, the 12 genes deviating most from their expected mutation burdens were exclusively affected by coding-direction *PB* insertions, including *MITF*, *MAP3K1/2*, and all recurrently mutated genes found in our screen. *MITF* is known to be amplified in melanoma, and we have already found that coding-direction *PB* insertions in *Mitf* and *Map3k1/2* resulted in pronounced up-regulation of gene expression (Fig. 1 *G* and *H*). These data suggest that aberrant activation of group II genes may be important for the development of melanoma.

To explore the possibility that group II genes are aberrantly activated in melanomas, we cross-referenced all 17 genes harboring coding-direction *PB* insertions with available somatic copy-number alteration and whole-transcriptome sequencing data from TCGA. Strikingly, 74% of 222 melanoma patients were affected by significant somatic copy-number alterations or mRNA expression changes in at least one of the genes. Remarkably, all 17 genes were nearly exclusively affected by recurrent gains (high-level amplifications or significant mRNA up-regulation) (Fig. 4 *D* and *E*). We further analyzed available microarray data by comparing the expression of these genes in 142 melanomas versus normal human melanocytes (40–42). Increased median-fold expression changes were observed for 65% of the genes (Fig. 4*E*). Notably, *MAP3K1* was the most highly up-regulated gene, providing patient-specific validation for our functional analysis of the recurrent *Map3k1* insertional mutations (Fig. 2). *ARHGEF3*, which was also recurrently mutated in our screen (Table 1), and *PRKDC* were prominently up-regulated as well (Fig. 4*E*). Thus, whereas group II genes are infrequently altered by somatic point mutations in melanoma and therefore unlikely to be deemed important by prevailing methods for detecting cancer-associated genes, they are aberrantly activated in a large number of patients and are likely to play previously unrecognized, functional roles in the development of melanoma.

Nine genes that are mutated at approximately the background mutation rate make up group III (Fig. 4*B*). These genes are indistinguishable from passengers on the basis of differential mutation frequency. Therefore, we were interested to ascertain whether the genes, having been implicated by low-copy *PB* mutagenesis as potentially important for melanomas, might actually be drivers that cannot be detected by iteratively sequencing tumors. We considered this possibility by examining whether the gene on this list with the lowest ratio of detected mutations versus passenger background (*PTPRO*; 0.77) might factor in cellular transformation (Fig. 4*B*). Because *Ptpro* transcript levels in the insertionally mutated mouse tumor were substantially reduced (Fig. 4*F*), we depleted *PTPRO* in p'mel-BRAF^{V600E} cells using lentivirus-mediated shRNA (Fig. 4*G*). Loss of *PTPRO* significantly promoted anchorage-independent colony growth in soft agar (Fig. 4*H* and Fig. S2). This result indicates that the low-copy *PB* mutagenesis approach can predict cancer-associated genes that are indistinguishable from background mutation rates.

Collectively, we have shown that the low-copy *PB* mutagenesis system is uniquely amenable to cross-species comparative analysis with hypermutated human sequencing data. By this analysis, our screen identified genes with a wide spectrum of mutation frequencies in human melanoma (high, low, and background levels). Although genes with low and background mutation frequencies are obscured from conventional cancer gene discovery approaches, we have established that these genes can be functionally significant in human melanomas. These results further demonstrate that the low-copy mutagenesis approach offers an unprecedented ability to interrogate novel melanoma-associated genes.

Discussion

It has been estimated that sequencing 2,500 tumor-normal pairs of the same cancer type may be necessary to overcome background mutation rates and identify somatically mutated driver genes in nonhypermutated cancers (1). However, a recent analysis of the heterogeneity found in cancer background mutation rates indicates that this number may be a considerable underestimation (14). Further accounting for the 10-fold higher mutation rates common in hypermutated cancers underscores the immense challenge of identifying driver genes by prevailing methods. In this paper, we have described a low-copy *PB* transposon mutagenesis system in mice for screening cancer-driving genes that circumvents the problematic background mutation rates in both human cancer and current transposon-based animal models. Using this approach, we were able to induce melanomas by an average of four insertional mutations instead of hundreds. This study represents a systematic interrogation of a solid tumor type by low-copy transposon insertional mutagenesis.

Although greatly different from human melanomas with respect to mutation rates, the melanomas generated by low-copy *PB* transposon mutagenesis nevertheless accurately recapitulate the genetic basis of human melanoma as we identified activating insertions in the melanoma oncogene *Mitf* and an inactivating insertion in the tumor suppressor *Cdkn2a*. Insertional mutations in known driver genes such as *Nras* and *Kit* were most likely not recovered given our choice of using an oncogenic *Braf* mutation (functioning downstream of *Nras* and *Kit*) at the outset of the screen. However, the loss of *Pten* is known to cooperate with oncogenic *Braf* in the genesis of melanoma (26), and the absence of insertional mutations in *Pten* from eleven *PB*-induced melanomas suggests that screening larger mutagenesis cohorts may be necessary to cover all known melanoma drivers. On the other hand, our identification of five recurrently mutated genes indicates that even a small cohort of mice undergoing low-copy somatic mutagenesis is sufficient to functionally implicate genes important in melanoma. These results predict that future low-copy transposon mutagenesis screens using larger cohorts of mice will uncover additional genes and pathways important for the initiation and progression of melanoma as well as other cancers.

Cross-species comparison between our list and human melanoma mutation data identified 11 genes that harbor high nonsilent mutation burdens, some that have been overlooked and others that are indistinguishable from passengers by conventional methods of cancer-gene discovery. For the two genes we characterized at greater depth, loss of *Magi2* expression and loss of *Ptpro* expression were prominent features of *Braf*^{V600E} melanomas harboring the respective insertional mutations, and, likewise, silencing of the orthologous genes in human *BRAF*^{V600E} melanocytes promoted cellular transformation. It is worth noting that MAGI2 interacts with a number of known cancer drivers including PTEN and β-catenin/CTNNB1 (35, 36) whereas the receptor-type protein tyrosine phosphatase PTPRO has been reported to interact with the melanoma driver KIT (43). Interestingly, the incidences of mutation in *PTEN*, *CTNNB1*, and *KIT* are all statistically underrepresented in human melanomas, emphasizing the importance of identifying drivers that may contribute to these pathways. Future studies are necessary to elucidate the specific mechanisms by which these new tumor suppressors exert their functional effects on melanoma.

Our study also uncovered a group of genes infrequently mutated in human melanomas yet nearly exclusively affected by high-level amplifications or up-regulation in a large percentage of melanoma patients. Mirroring these alterations, orthologous genes from the low-copy mutagenesis screen harbored coding-direction *PB* mutations in 5′ regulatory regions or introns, which are predicted to drive gene expression. Indeed, seven such coding-direction insertions were verified to drive the expression of

Mitf, *Map3k1*, and *Map3k2*. The striking up-regulation of these genes observed both in our screen and in human melanomas indicates that the low-copy *PB* system can be advantageously harnessed to interrogate putative protooncogenes that may be infrequently activated by somatic point mutations in human cancers.

In this group, *MAP3K1* was the most highly up-regulated gene compared with human melanocytes, and its potential importance was recapitulated by recurrent insertional mutations driving *Map3k1* expression in mouse tumors. Because most of the mutations were mutually exclusive with $Braf^{V600E}$, aberrant *MAP3K1* expression may contribute to melanoma initiation in patients without oncogenic alterations in *BRAF*, *NRAS*, or *KIT*, and this possibility is supported by the activation of ERK signaling and conferral of cancer hallmarks in human melanocytes. Pharmacological studies building on these findings will help determine whether dysregulation of *MAP3K1* might also contribute to melanoma relapse and resistance following BRAF-targeted therapy. Moreover, although our screen indicates that partial *MAP3K1* gene products can drive tumorigenesis in mice, the nature of alterations leading to aberrant *MAP3K1* expression in human patients remains to be determined. Interestingly, the existence of similar alterations in human melanomas is established. A recent study found that aberrant splicing of *BRAF*, leading to the removal of multiple exons at the 5′ end of the transcript, occurs in ∼30% of patients surveyed and generates constitutively active truncated gene products (44). Although a clearer picture will be gained from more extensive characterization of *MAP3K1* alterations in human melanomas, our study demonstrates that the low-copy *PB* approach provides predictive power for potential melanoma-associated genes that cannot be discovered by purely sequencing tumors and has made compelling inroads for further exploration in this area.

Overall, we have shown that the low-copy *PB* mutagenesis system generates biologically meaningful results whereby the genetic alterations are highly relevant to the tumor. Our study represents a conceptual advance from previous high-copy transposon mutagenesis screens and provides proof-of-principle to a powerful, unique approach that facilitates unbiased discovery of cancer-driving genes. Moreover, we identified *MAGI2*, *PTPRO*, and *MAP3K1* as previously undescribed melanoma-associated genes and uncovered a functional role for aberrant *MAP3K1* expression in promoting melanocyte growth factor autonomy. Further functional investigation of the candidate genes identified in this study is warranted to determine their biological roles in human melanoma.

Materials and Methods

Mice. Animal experiments were approved and conducted in compliance with the Yale Animal Resources Center and Institutional Animal Care and Use Committee under the protocol 2008–10230. *Act-PBase* (linked to the *K14-Tyr* transgene) and *Luc-PB[mut]7* (linked to the *αA-tdTomato* transgene) mice were genotyped by coat color and lens fluorescence, respectively (16, 19). $Braf^{CA}$ and *Tyr-CreER* mice were genotyped by PCR using primer sequences previously described (27, 28). *Act-PBase* and *Luc-PB[mut]7* mice were crossed separately to $Braf^{CA}$*;Tyr-CreER* mice to generate triple transgenic lines. Subsequent crosses between the triple transgenic lines were made to obtain quadruple transgenic mice for the mutagenesis cohort ($Braf^{CA}$*;Tyr-CreER; Luc-PB[mut]7;Act-PBase*) and triple transgenic mice for the nonmutagenesis control cohorts ($Braf^{CA}$*;Tyr-CreER;Luc-PB[mut]7* and $Braf^{CA}$*;Tyr-CreER;Act-PBase* littermates). Mutagenesis and nonmutagenesis cohorts were maintained on a mixed C57BL/6J and FVB/NJ background. To activate CreER, we administered 1 mg of tamoxifen-in-sunflower seed oil to mutagenesis and control mice for 5 consecutive days by i.p. injection. Over the course of the screen, mice were imaged using the IVIS Spectrum (PerkinElmer), requiring isoflurane anesthesia delivered by a precision vaporizer [2.5% (vol/vol) isoflurane in oxygen] and i.p. injection with 1.5 mg of luciferin (dissolved in PBS) per 10 g of body weight.

Mapping Insertional Mutations. We performed linker-mediated PCR to amplify genomic sequences flanking *PB* insertions as previously described (19), with modifications starting at the secondary amplification step to permit multiplexed Illumina sequencing. The custom primers enabling multiplexed Illumina sequencing can be found in Table S3. After sequencing the PCR products, paired-end reads were demultiplexed and mapped against the reference genome using Illumina's standard Casava pipeline (version 1.8.2). A custom python script was used to find and count the number of Read1 reads mapping to each unique location (including orientation of *PB* insertion) in the genome. We calculated statistics on the paired-end insert size for each location and annotated each position with the genes immediately up- and downstream, using as gene annotations refFlat.txt from goldenPath at the University of California, Santa Cruz (http://genome.ucsc.edu/). A 15-Mb local transposition window on chromosome 1 was observed and discounted from further analysis. Insertional mutations (encompassing insertions that occurred in exons, introns, or 4 kb upstream of first exons) that contributed to high read counts in samples (≥5% of the most abundant insertion's read count) were deemed likely to be present in the dominant tumor clone and drive tumorigenesis. PCR verification of insertional mutations was performed using primers specific to the *PB* transposon (5′-AAATCAGTGACACTTACCGCATTGACAAG-3′ and 5′-CCTCTAATAGTCCTCTGTGGCAAGGTCAAG-3′) and to the mouse genomic DNA flanking the insertion sites (Table S3).

RT-PCR. Macrodissected tissue was homogenized using a bead mill homogenizer (Qiagen); cell lysates were homogenized by passing through a 20-gauge syringe. Purified RNA was used in the iScript reaction (Bio-Rad) to synthesize cDNA. RT-PCR was performed using primer pairs that span splicing junctions between the *PB[mut]* initiator exon and downstream exons of inserted genes. The primer for the *PB[mut]* initiator exon was 5′-TGGGGAATGGAGCAGAAGCTC-3′. Primers used for exons downstream of the insertion site were 5′-ATAAGCAGCCAACGAGTTCC-3′ and 5′-TACCAGCATGGCTCTCAATG-3′ (*Map3k1*), and 5′-CCACAGCTTTGTCCAAGTCA-3′ (*Map3k2*). Products were sequenced to confirm transposon-derived chimeric mRNA. qPCR with SYBR green (Applied Biosystems) was performed in triplicate for each sample to determine gene expression using the relative standard-curve method. For determining up-regulation or down-regulation of each gene in bulk mouse tumors, relative transcript levels in melanomas harboring the insertional mutations of interest were compared with three melanomas without the insertional mutations, and *P* values were calculated using the *t* test. Primer pairs used can be found in Table S3.

Histology and Immunohistochemistry. Melanomas were fixed overnight in 10% neutral-buffered formalin and dehydrated with a series of ethanol and xylenes. Paraffin-embedded sections were stained with hematoxylin and eosin. For immunohistochemistry, sections were deparaffinized and rehydrated before heat-induced antigen retrieval in sodium citrate and subsequently incubated with the primary antibodies MAP3K1 (Millipore; 07–1476) or S100 (Thermo Scientific; RB-044-A1). Slides were developed using a diaminobenzidine-peroxidase substrate kit (Vector Labs) and counterstained with hematoxylin.

Cell Culture. The 293T cells were cultured in DMEM supplemented with 10% FBS; YUMAC melanoma cells (32) were cultured in OptiMEM supplemented with 10% FBS; immortalized human melanocytes (p'mel) (33) were cultured in Medium 254 supplemented with 1% L-glutamine and HMGS (Invitrogen); p'mel cells expressing $BRAF^{V600E}$ (p'mel-$BRAF^{V600E}$) (33) were cultured in DMEM/F12 growth medium supplemented with 10% FBS and 1% L-glutamine. Truncations of *Map3k1* were generated by PCR amplification using full-length rat *Map3k1* cDNA as template (45) and subsequently cloned into the *pCEP4* expression vector. Subconfluent HEK293T cells in 60-mm dishes were transfected with 8 μg of expression plasmid for $Map3k1^{FL}$, $Map3k1^{\Delta 1}$, $Map3k1^{\Delta 2}$, or control *RFP* using Lipofectamine 2000 (Invitrogen) and harvested 24 h after transfection for protein analysis. For experiments with PLX4032, subclonfluent YUMAC cells in 60-mm dishes were transfected with 8 μg of expression plasmid for $Map3k1^{\Delta 1}$, $Map3k1^{\Delta 2}$, or control *RFP* using FuGENE HD (Roche). Twenty hours posttransfection, cells were treated with either 0.1% DMSO or 1 μM PLX4032 for 4 h before harvesting for protein analysis.

Western Blotting. Cell lysis was carried out in Nonidet P-40 buffer with protease and phosphatase inhibitors at 4 °C (Roche). Total protein was quantified by the BCA Assay (Pierce). Protein samples were separated by SDS/PAGE according to standard Western blotting procedures and transferred to nitrocellulose membranes (Bio-Rad), followed by blocking with 5% skim milk for 1 h. Blots were incubated with primary antibodies to MAP3K1 (Millipore; 07–1476), ERK1/2 (Cell Signaling; 9102), phospho-ERK1/2 (Cell Signaling; 9101), MAGI2 (Santa Cruz; sc-25664), and ACTB (Cell Signaling; 3700) overnight at 4 °C. Anti-mouse and anti-rabbit secondary antibodies conjugated

to horseradish peroxidase were used for protein detection, and signal was visualized using enhanced chemiluminescence (Perkin-Elmer). Quantification of protein levels was performed by densitometric analysis of immunoblots using the ImageJ program (National Institutes of Health).

Lentivirus Production. shRNAs specific for *MAGI2* (TRCN0000148546 and TRCN0000240506) and *PTPRO* (TRCN0000002901 and TRCN0000002904) were cloned into *pLKO.1-blast* (46). *Map3k1*$^{\Delta 1}$ was cloned into *pCS-CG* (47). Lentiviruses were produced by overnight triple cotransfection of HEK293T cells using FuGENE HD and 4 μg of Δ8.9, 2 μg of VSV-G, and 4 μg of expression vector. p'mel-BRAF^{V600E} cells were incubated overnight with 48- and 72-h posttransfection viral supernatants supplemented with polybrene and then blasticidin-selected for 1 wk before use in functional assays. p'mel human melanocytes were incubated overnight with 48-h posttransfection viral supernatants supplemented with polybrene and directly used in functional assays.

Soft Agar Assays. The p'mel-BRAF^{V600E} cells expressing shRNA for *MAGI2*, *PTPRO*, or a scramble control were seeded in six-well plates at 10^4 cells per well in 0.4% SeaPlaque agarose in DMEM/F12 with 10% FBS and layered onto 0.8% agarose in DMEM/F12 with 10% FBS. Two independent shRNA constructs were used for each gene. Soft agar experiments were performed in triplicate. Colonies were imaged, stained with 0.005% crystal violet, and quantified (colonies $\geq$ 100 μm diameter) after 3 wk. Data are presented as the average number of colonies per well, and *P* values were calculated using the *t* test.

Growth Factor Autonomy Assays. The 10^4 p'mel cells per well of 12-well plates were transduced with lentivirus expressing either empty vector (EV) or Map3k1$^{\Delta 1}$, were cultured in growth factor-deprived medium (DMEM/F12 medium with 10% FBS and 1% L-glutamine) 24-h postinfection, and were maintained under growth-factor deprivation for 2 wk. Three independent experiments were performed. Brightfield images of cells were taken over the course of the experiment. At the end point, cells were fixed in 4% paraformaldehyde, stained with a 0.1% solution of crystal violet, washed extensively, and air dried. Bound dye was recovered using 10% acetic acid, and absorbance at 595 nm was measured by a plate reader. Cell numbers as determined by absorbance values were calculated by the relative standard curve method. Data are presented as the average number of cells per well, and *P* values were calculated using the *t* test.

Analysis of Protein Interaction Networks. The Search Tool for the Retrieval of Interacting Genes/Proteins (STRING; http://string-db.org/) with a threshold confidence setting of 0.6 was used to build networks of experimentally validated human protein associations (48).

Statistical Analysis of Nonsilent Mutation Burden. Melanoma somatic mutation data were downloaded from independent studies (6–11) and TCGA data portal. The probability of random mutation occurring in any given gene was calculated based on the size of the gene and the average number of nonsilent mutations in human melanoma. The average number of mutations in melanoma was determined by the sample number-weighted average of mutations reported in melanoma exome-sequencing studies (6–11). RefSeq gene sizes were used in calculations. Calculations were performed under the following assumptions: first, the probability of mutation at all possible positions of the exome is equal; second, each gene is mutated once per tumor; and third, mutational events are independent. A χ^2 goodness-of-fit test was performed to evaluate the null hypothesis, which states that the observed mutational frequency of a gene across 570 melanoma patients occurs without positive somatic selection.

Analysis of Somatic Copy Number Alteration and Gene Expression Data. Somatic copy number alteration data and whole transcriptome sequencing data for 17 genes from 222 melanoma patients were generated by TCGA and analyzed using the cBioPortal for Cancer Genomics (http://www.cbioportal.org/) (49, 50). For determination of significant somatic copy number alterations, GISTIC scores of 2 (high-level amplification) or −2 (deep loss) were considered. For determination of mRNA up-regulation or down-regulation, a z-score threshold of ±2 was considered a significant deviation from the mean melanoma expression level. A gene was considered recurrently gained if the ratio of patient samples with significant amplification or mRNA up-regulation to those with significant loss or mRNA down-regulation was greater than 1.5. Eleven of 17 genes were exclusively amplified or up-regulated, 5 of the remaining 6 genes had ratios greater than 5, and *SH3BP4* had a ratio of 1.7. Microarray data from independent studies comparing human melanomas versus normal melanocytes were downloaded from Oncomine (www.oncomine.com/) (51). Sample number-weighted averages of the median-fold changes in melanomas relative to normal melanocytes were calculated for each gene.

ACKNOWLEDGMENTS. We thank Martin McMahon for *Braf*^{CA} mice, Melanie Cobb for *Map3k1* cDNA, Hans Widlund for p'mel cells, John Overton for Illumina sequencing, Yale Specialized Programs of Research Excellence in Skin Cancer and Ruth Halaban for YUMAC cells, Plexxikon for PLX4032, The Cancer Genome Atlas for multiplatform data on melanoma, Charlotte Kuperwasser for support during the performance of revisions, and Mingzi Zhang, Jinyu Lu, Anna Vilborg, Jade Li, Ming Wu, Thomas Klein, and Shih-Chieh Ti for critical reading of the manuscript. This work was supported by the Howard Hughes Medical Institute. T.K.N. was supported by Genetics Training Grant T32 GM007499 and Training Program in Genomics and Proteomics Technologies Grant T32 HG003198 from the National Institutes of Health. S.F.L. was supported by American Cancer Society Fellowship PF-08-256-01-GMC and an Alex's Lemonade Stand Young Investigator Award.

1. Garraway LA, Lander ES (2013) Lessons from the cancer genome. *Cell* 153(1):17–37.
2. Kumar A, et al. (2011) Exome sequencing identifies a spectrum of mutation frequencies in advanced and lethal prostate cancers. *Proc Natl Acad Sci USA* 108(41):17087–17092.
3. Cancer Genome Atlas Network (2012) Comprehensive molecular characterization of human colon and rectal cancer. *Nature* 487(7407):330–337.
4. Cancer Genome Atlas Network (2012) Comprehensive molecular portraits of human breast tumours. *Nature* 490(7418):61–70.
5. Pleasance ED, et al. (2010) A comprehensive catalogue of somatic mutations from a human cancer genome. *Nature* 463(7278):191–196.
6. Wei X, et al.; NISC Comparative Sequencing Program (2011) Exome sequencing identifies GRIN2A as frequently mutated in melanoma. *Nat Genet* 43(5):442–446.
7. Stark MS, et al. (2012) Frequent somatic mutations in MAP3K5 and MAP3K9 in metastatic melanoma identified by exome sequencing. *Nat Genet* 44(2):165–169.
8. Nikolaev SI, et al. (2012) Exome sequencing identifies recurrent somatic MAP2K1 and MAP2K2 mutations in melanoma. *Nat Genet* 44(2):133–139.
9. Berger MF, et al. (2012) Melanoma genome sequencing reveals frequent PREX2 mutations. *Nature* 485(7399):502–506.
10. Hodis E, et al. (2012) A landscape of driver mutations in melanoma. *Cell* 150(2): 251–263.
11. Krauthammer M, et al. (2012) Exome sequencing identifies recurrent somatic RAC1 mutations in melanoma. *Nat Genet* 44(9):1006–1014.
12. Cancer Genome Atlas Research Network (2012) Comprehensive genomic characterization of squamous cell lung cancers. *Nature* 489(7417):519–525.
13. Imielinski M, et al. (2012) Mapping the hallmarks of lung adenocarcinoma with massively parallel sequencing. *Cell* 150(6):1107–1120.
14. Lawrence MS, et al. (2013) Mutational heterogeneity in cancer and the search for new cancer-associated genes. *Nature* 499(7457):214–218.
15. Ivics Z, Hackett PB, Plasterk RH, Izsvák Z (1997) Molecular reconstruction of Sleeping Beauty, a Tc1-like transposon from fish, and its transposition in human cells. *Cell* 91(4):501–510.
16. Ding S, et al. (2005) Efficient transposition of the piggyBac (PB) transposon in mammalian cells and mice. *Cell* 122(3):473–483.
17. Copeland NG, Jenkins NA (2010) Harnessing transposons for cancer gene discovery. *Nat Rev Cancer* 10(10):696–706.
18. Rad R, et al. (2010) PiggyBac transposon mutagenesis: A tool for cancer gene discovery in mice. *Science* 330(6007):1104–1107.
19. Landrette SF, Cornett JC, Ni TK, Bosenberg MW, Xu T (2011) piggyBac transposon somatic mutagenesis with an activated reporter and tracker (PB-SMART) for genetic screens in mice. *PLoS ONE* 6(10):e26650.
20. March HN, et al. (2011) Insertional mutagenesis identifies multiple networks of cooperating genes driving intestinal tumorigenesis. *Nat Genet* 43(12):1202–1209.
21. Mann KM, et al.; Australian Pancreatic Cancer Genome Initiative (2012) Sleeping Beauty mutagenesis reveals cooperating mutations and pathways in pancreatic adenocarcinoma. *Proc Natl Acad Sci USA* 109(16):5934–5941.
22. Pérez-Mancera PA, et al.; Australian Pancreatic Cancer Genome Initiative (2012) The deubiquitinase USP9X suppresses pancreatic ductal adenocarcinoma. *Nature* 486(7402):266–270.
23. Flaherty KT, Hodi FS, Fisher DE (2012) From genes to drugs: Targeted strategies for melanoma. *Nat Rev Cancer* 12(5):349–361.
24. Davies H, et al. (2002) Mutations of the BRAF gene in human cancer. *Nature* 417(6892):949–954.
25. Pollock PM, et al. (2003) High frequency of BRAF mutations in nevi. *Nat Genet* 33(1): 19–20.
26. Dankort D, et al. (2009) Braf(V600E) cooperates with Pten loss to induce metastatic melanoma. *Nat Genet* 41(5):544–552.
27. Dankort D, et al. (2007) A new mouse model to explore the initiation, progression, and therapy of BRAFV600E-induced lung tumors. *Genes Dev* 21(4):379–384.
28. Bosenberg M, et al. (2006) Characterization of melanocyte-specific inducible Cre recombinase transgenic mice. *Genesis* 44(5):262–267.
29. Blank JL, Gerwins P, Elliott EM, Sather S, Johnson GL (1996) Molecular cloning of mitogen-activated protein/ERK kinase kinases (MEKK) 2 and 3. Regulation of sequential phosphorylation pathways involving mitogen-activated protein kinase and c-Jun kinase. *J Biol Chem* 271(10):5361–5368.

30. Karandikar M, Xu S, Cobb MH (2000) MEKK1 binds raf-1 and the ERK2 cascade components. *J Biol Chem* 275(51):40120–40127.
31. Lu Z, Xu S, Joazeiro C, Cobb MH, Hunter T (2002) The PHD domain of MEKK1 acts as an E3 ubiquitin ligase and mediates ubiquitination and degradation of ERK1/2. *Mol Cell* 9(5):945–956.
32. Halaban R, et al. (2010) PLX4032, a selective BRAF(V600E) kinase inhibitor, activates the ERK pathway and enhances cell migration and proliferation of BRAF melanoma cells. *Pigment Cell Melanoma Res* 23(2):190–200.
33. Garraway LA, et al. (2005) Integrative genomic analyses identify MITF as a lineage survival oncogene amplified in malignant melanoma. *Nature* 436(7047):117–122.
34. Ohtsuka T, et al. (1999) nRap GEP: A novel neural GDP/GTP exchange protein for rap1 small G protein that interacts with synaptic scaffolding molecule (S-SCAM). *Biochem Biophys Res Commun* 265(1):38–44.
35. Nishimura W, Yao I, Iida J, Tanaka N, Hata Y (2002) Interaction of synaptic scaffolding molecule and β -catenin. *J Neurosci* 22(3):757–765.
36. Tolkacheva T, et al. (2001) Regulation of PTEN binding to MAGI-2 by two putative phosphorylation sites at threonine 382 and 383. *Cancer Res* 61(13):4985–4989.
37. Berger MF, et al. (2011) The genomic complexity of primary human prostate cancer. *Nature* 470(7333):214–220.
38. Banerji S, et al. (2012) Sequence analysis of mutations and translocations across breast cancer subtypes. *Nature* 486(7403):405–409.
39. Bamford S, et al. (2004) The COSMIC (Catalogue of Somatic Mutations in Cancer) database and website. *Br J Cancer* 91(2):355–358.
40. Hoek K, et al. (2004) Expression profiling reveals novel pathways in the transformation of melanocytes to melanomas. *Cancer Res* 64(15):5270–5282.
41. Hoek KS, et al. (2006) Metastatic potential of melanomas defined by specific gene expression profiles with no BRAF signature. *Pigment Cell Res* 19(4):290–302.
42. Riker AI, et al. (2008) The gene expression profiles of primary and metastatic melanoma yields a transition point of tumor progression and metastasis. *BMC Med Genomics* 1:13.
43. Taniguchi Y, London R, Schinkmann K, Jiang S, Avraham H (1999) The receptor protein tyrosine phosphatase, PTP-RO, is upregulated during megakaryocyte differentiation and Is associated with the c-Kit receptor. *Blood* 94(2):539–549.
44. Poulikakos PI, et al. (2011) RAF inhibitor resistance is mediated by dimerization of aberrantly spliced BRAF(V600E). *Nature* 480(7377):387–390.
45. Xu S, et al. (1996) Cloning of rat MEK kinase 1 cDNA reveals an endogenous membrane-associated 195-kDa protein with a large regulatory domain. *Proc Natl Acad Sci USA* 93(11):5291–5295.
46. Bryant DM, et al. (2010) A molecular network for de novo generation of the apical surface and lumen. *Nat Cell Biol* 12(11):1035–1045.
47. Miyoshi H, Blömer U, Takahashi M, Gage FH, Verma IM (1998) Development of a self-inactivating lentivirus vector. *J Virol* 72(10):8150–8157.
48. Szklarczyk D, et al. (2011) The STRING database in 2011: Functional interaction networks of proteins, globally integrated and scored. *Nucleic Acids Res* 39(Database issue):D561–D568.
49. Cerami E, et al. (2012) The cBio cancer genomics portal: An open platform for exploring multidimensional cancer genomics data. *Cancer Discov* 2(5):401–404.
50. Gao J, et al. (2013) Integrative analysis of complex cancer genomics and clinical profiles using the cBioPortal. *Sci Signal* 6(269):pl1.
51. Rhodes DR, et al. (2007) Oncomine 3.0: Genes, pathways, and networks in a collection of 18,000 cancer gene expression profiles. *Neoplasia* 9(2):166–180.